



Article

Retrieval of Chlorophyll-a Concentrations of Class II Water Bodies of Inland Lakes and Reservoirs Based on ZY1-02D Satellite Hyperspectral Data

Li Lu ^{1,2}, Zhaoning Gong ^{1,2,*} , Yanan Liang ^{1,2} and Shuang Liang ^{1,2}

¹ College of Resources, Environment and Tourism, Capital Normal University, Beijing 100048, China; 2190902128@cnu.edu.cn (L.L.); 2190902148@cnu.edu.cn (Y.L.); liangs@cnu.edu.cn (S.L.)

² Beijing Municipal Key Laboratory of Resources Environment and GIS, Beijing 100048, China

* Correspondence: gongzhn@cnu.edu.cn

Abstract: Chlorophyll-a is an important parameter that characterizes the eutrophication of water bodies. The advantage of ZY1-02D hyperspectral satellite subdivision in the visible light and near-infrared bands is that it highlights the unique characteristics of water bodies in the spectral dimension, and it helps to assess the Class II water bodies of inland lakes and reservoirs, making it an important tool for refined remote sensing detection of the environment. In this study, the Baiyangdian Nature Reserve in northern China, which contains a typical inland lake and wetland, was chosen as the study area. Using ZY1-02D hyperspectral synchronization transit images and in situ measured chlorophyll-a concentration as the data source, remote sensing of the chlorophyll-a concentration of inland lakes was conducted. By analyzing the correlation between the spectral reflectance of the ZY1-02D hyperspectral image and the chlorophyll-a concentration and using algorithms such as the single band, band ratio, and three bands to compare and filter characteristic wavelengths, a quantitative hyperspectral model of the chlorophyll-a concentration was established to determine the chlorophyll-a concentration of Baiyangdian Lake. The dynamic monitoring of the water body and the assessment of the nutritional status of the water body were determined. The results revealed that the estimation of the chlorophyll-a concentration of Baiyangdian Lake based on the hyperspectral Fluorescence Line Height (FLH) model was ideal, with an R^2 value of 0.78. The FLH model not only comprehensively considers the effects of suspended solids, yellow substances, and backscattering of the water body on the estimation of the chlorophyll-a concentration, but also considers the influence of the elastic scattering efficiency of the chlorophyll. Based on the ZY1-02D hyperspectral data, a spatial distribution map of the chlorophyll-a concentration of Baiyangdian Lake was created to provide new ideas and technical support for monitoring inland water environments.

Keywords: ZY1-02D hyperspectral imagery; chlorophyll-a concentration; retrieval; Baiyangdian wetlands



Citation: Lu, L.; Gong, Z.; Liang, Y.; Liang, S. Retrieval of Chlorophyll-a Concentrations of Class II Water Bodies of Inland Lakes and Reservoirs Based on ZY1-02D Satellite Hyperspectral Data. *Remote Sens.* **2022**, *14*, 1842. <https://doi.org/10.3390/rs14081842>

Academic Editors: Dionissios Kalivas, Christos Chalkias, Thomas Alexandridis, Konstantinos X. Soulis and Emmanouil Psomiadis

Received: 11 March 2022

Accepted: 9 April 2022

Published: 12 April 2022

Publisher's Note: MDPI stays neutral with regard to jurisdictional claims in published maps and institutional affiliations.



Copyright: © 2022 by the authors. Licensee MDPI, Basel, Switzerland. This article is an open access article distributed under the terms and conditions of the Creative Commons Attribution (CC BY) license (<https://creativecommons.org/licenses/by/4.0/>).

1. Introduction

Chlorophyll-a is a pigment contained in all algae. It is an important indicator of the degree of eutrophication of water bodies and it is also monitored in Chinese aquatic environments [1]. It is difficult for traditional water quality monitoring based on on-site sampling and laboratory measurements to capture the temporal and spatial distributions of chlorophyll-a. In comparison, remote sensing technologies have many advantages, including the following: rapidity, ease of access, and large-scale, exhaustive coverage [2]. It can be an effective method of achieving long-term and large-scale monitoring of water eutrophication [3]. In consequence, a series of chlorophyll-a concentration inversion algorithms have been developed [4].

The quantitative inversion of the chlorophyll-a concentration is an important remote sensing method used to assess the nutritional status of water bodies. For example, with ocean-

based Type I water bodies, the chlorophyll-a concentration inversion algorithm is highly accurate and widely applied [5]. However, there are approximately 2693 lakes and reservoirs in China with areas greater than 1 km². Up to 74% of China's lakes and reservoirs have areas less than 10 km² [6]. Small- and medium-sized lakes and reservoirs are important components of inland and nearshore Class II water bodies. Inland and nearshore Class II water bodies are most closely associated with a human presence and activities. For Class II water bodies, the model has a weak adaptability, uncertainty, and low accuracy.

Currently, the commonly used satellite sensors for chlorophyll-a data retrieval for small- and medium-sized inland lakes and reservoirs include: EO-1 Hyperion, Medium Resolution Imaging Spectrometer (MERIS), Moderate Resolution Imaging Spectroradiometer (MODIS), Visible Infrared Imaging Radiometer Suite (VIIRS), Landsat, Sentinel, and Unmanned Aerial Vehicles (UAVs) [7]. For example, Feng et al. (2015) used MERIS data to invert the chlorophyll-a concentration of Poyang Lake and discussed the temporal and spatial distributions of the chlorophyll-a concentration and eutrophication issues [8]. Jiang Guangjia et al. (2020) used VIIRS data to analyze chlorophyll-a in inland and coastal waters [9]. Li Yunmei et al. (2021) used the Ocean and Land Color Instrument (OLCI) data optical fuzzy clustering algorithm to evaluate the single chlorophyll-a algorithm [10]. However, the lower spatial resolution of water-color satellites cannot accurately extract small and medium lake water bodies, which limits the inversion of chlorophyll-a concentration.

Based on Hyperion hyperspectral data, Du Cong et al. (2009) used the three-band method to retrieve the chlorophyll-a concentration of Lake Tai [11]. Yin Ziyao et al. (2021) used the Zhuhai-1 hyperspectral satellite to retrieve the parameters of the Qiao Reservoir, proving that the satellite-to-ground synchronous hyperspectral experiment has the potential to quantitatively retrieve water quality parameters [12]. Hyperion sensors and other hyperspectral sensors have the advantages of high spectral and spatial resolutions. There are advantages in terms of their resolution, but their low signal-to-noise ratio and limited acquisition methods limit their application in inland water chlorophyll-a retrieval. The diversity of remote sensing data sources available and the improvement of their spatial resolution have permitted investigations of the chlorophyll-a inversion in inland and coastal water bodies under a range of circumstances. For example, Nima Pahlevan et al. (2020) used Sentinel-2 and Sentinel-3 data [13], Wang Xing et al. (2018) used Worldview data [14], and Yingying Gai et al. (2020) used UAV airborne sensors to investigate the inversion of the chlorophyll-a concentrations of inland and coastal water bodies [15]. The difficulty of acquiring airborne satellite data and the high cost of acquiring high spatial resolution satellites hinder its application in the retrieval of chlorophyll-a concentration data. James Bramich et al. (2021) used Sentinel-2 to improve the red edge algorithm and created an inversion algorithm for the chlorophyll-a concentration [16]. Cao Zhigang et al. (2020) used Landsat-8 to explore the method of inverting the chlorophyll-a concentrations of Lakes in the middle reaches of the Yangtze River [17]. Nonetheless, it remains difficult for multi-spectral data with a wide band to accurately capture the spectral characteristics of chlorophyll-a in inland water bodies, while the accuracy of inverting the chlorophyll-a concentration is often not high and the stability is poor.

Currently, China's latest ZY-02D satellite belongs to a new generation of hyperspectral imaging technology. It is equipped with both a high spectral resolution sensor (AHSI) and a high spatial resolution sensor (VNIC) [18]. The spectral resolution sensor (AHSI) has spectral resolutions of 10 nm and 20 nm in the Visible and Near (VN) infrared and Short-Wave (SW) infrared bands, and it has 166 bands. The signal-to-noise ratio of the data is better than that of previous hyperspectral data, such as EO-1 Hyperion and HJ-1 Hyper Spectral Imager (HSI) data. Therefore, it could be suitable for inland areas and in the monitoring of the water body parameters of small lakes and reservoirs.

As the largest freshwater lake in the North China Plain, Baiyangdian Lake is characterized by a vast amount of water, complex ground cover types, and strong human influence [19]. The water environment of a lake can reflect the health of the regional ecology to a certain extent. The chlorophyll-a concentration is representative of the pri-

many productivity and richness of the water body, as well as an important indicator of the degree of nutrition. In this study, a combination of Baiyangdian ZY1-02D image data and measured chlorophyll-a data were used to compare and analyze the commonly used chlorophyll-a concentration inversion algorithm and to construct a chlorophyll-a inversion algorithm for Baiyangdian Lake. The objective was to be able to provide suggestions for the eutrophication management of Baiyangdian Lake and guidance for the Xiong'an district

2. Materials

2.1. Study Area

Baiyangdian Lake is located in Anxin County, Xiong'an New District, Hebei Province (Figure 1). It is known as the “Pearl of North China” and is the largest shallow lake wetland in the North China Plain. The water in Baiyangdian Lake is supplied by nine rivers in the Daqing River system and is also called the “nine rivers under the tip” [20]. In modern geography, these nine rivers are the Zhulong River, Xiaoyi River, Tang River, Qingshui River, Baohe River, Fuhe River, Ping River, Caohe River, and Baigou River. In contrast to other Chinese large lakes and reservoirs such as Taihu Lake, Chaohu Lake, and Guanting Reservoir, Baiyangdian Lake is characterized by a complex topography, with many connected rivers and ravines. More than 3700 channels and waterways connect 143 lakes of different sizes to form reed fields and garden terraces, creating a unique natural landscape consisting of a mosaic of depressions and villages. The total area of Baiyangdian Lake is 366 km². There are more than 6 million square meters of lakes, including Baiyangdian Lake, Shaoche Lake, Mapeng Lake, Yangjiao Lake, Chiyu Lake, Houtang Lake, and Xiaobeidian Lake. There are 24 lakes with areas of 10,000 m², and 112 lakes with areas of less than 600,000 m². Among all of these lakes, Baiyangdian Lake has the largest area, so this conglomeration of lakes is referred to as Baiyangdian Lake. With the establishment of the Xiong'an New District, industries have developed rapidly in the upper reaches of Baiyangdian, causing serious water pollution. The main problems include reduced water inflow, insufficient water storage, a low water retention capacity, and poor water self-purification [21].

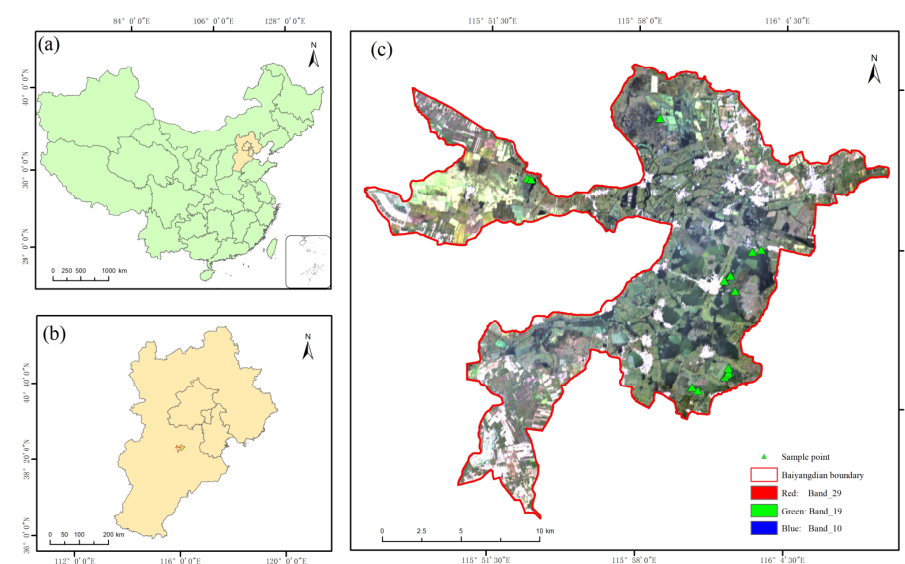


Figure 1. Maps of the study area (a) China, (b) Beijing-Tianjin-Hebei Province, (c) study sites at Baiyangdian Lake.

2.2. In Situ Survey Data

2.2.1. In Situ Chlorophyll-a Data

In this study, 21 sets of water quality sample data were collected simultaneously in Baiyangdian on 7 October 2020 according to ZY1-02D transit time, and the sampling points are shown in Figure 1. A Hach Hydrolab MS5 multi-probe water quality measuring

instrument was used to conduct the on-site water quality measurements. The MS5 multi-probe can simultaneously measure the water temperature, Total Dissolved Solids (TDSs), chlorophyll-a (Chl-a), turbidity, and other parameters. The water quality was measured for 10 s at each sampling point, three replicate sets of measures were obtained at each sampling point. The average value was used in subsequent analysis.

2.2.2. In Situ Remote Sensing Reflectance Data

The research team carried out satellite-ground synchronous observation experiments in the study area according to the transit time of the satellite to obtain a water-color matching dataset. An ASD FieldSpec3 portable field hyperspectral ground spectrometer was used. The spectrum was collected under dry, windless, clear, and cloudless or less cloudy conditions, and the standard board (25% gray board) was corrected in time according to the weather conditions. The measurement time was taken during the period (10:00–14:00) when the Sun's altitude angle was greater than 45° . The measurement of the water spectrum was conducted following the international standard by measuring above the water surface [22].

$$R_{rs} = \frac{[S_{sw} - rS_{sky}] \rho_p}{\pi S_p} \quad (1)$$

where R_{rs} is the spectral reflectance value of the water body; S_{sw} , S_{sky} , and S_p are the measured signal values when the spectrometer was facing the water, the sky, and the standard plate, respectively; and r is the reflectance of the air-water interface. Based on previous studies, $r = 2.2\%$ for calm water. ρ_p is the reflectivity of the standard plate.

To obtain a ZY1-02D satellite-ground synchronously measured reflectance dataset for Baiyangdian, the following two principles were followed to match the reflectivity R_{rs} of the sampling point and the corresponding ZY1-02D satellite image pixel. Spatially, it was ensured that the position of the pixel and the ground point were consistent. In addition, it was necessary to ensure that the pixel had a good uniformity, and the ratio of the standard deviation of the 3×3 neighborhood pixel value around the pixel to the mean value did not exceed 0.4. Temporally, it was ensured that the time interval between the pixel and the measured point was no more than 5 days. Therefore, the research team measured 8 sets of spectral data of water bodies in Baiyangdian on 7 October 2020. Each set of data was measured with 10 spectral curves, with curve processing including spectral smoothing, denoising, and averaging. The measured spectral curves were obtained as shown in Figure 2.

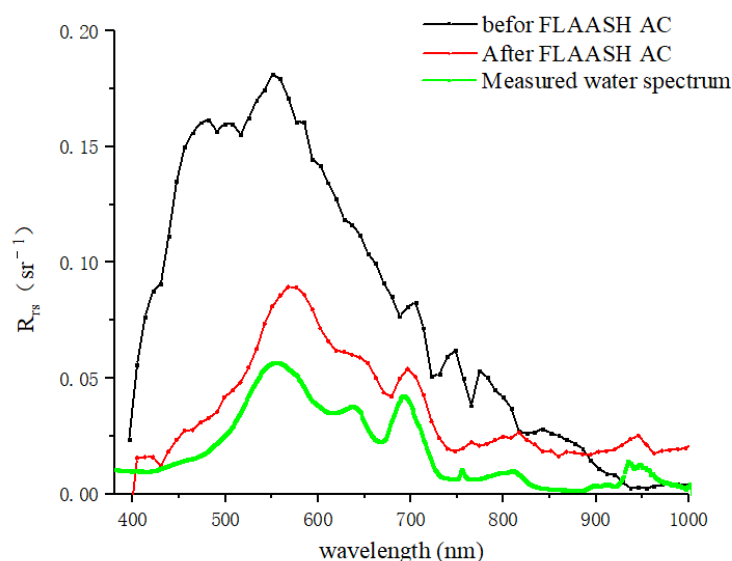


Figure 2. Comparison of the in situ measured water spectrum with the spectrum of the water bodies before and after atmospheric correction of the same pixel.

2.3. ZY1-02D Image Data

The ZY1-02D satellite is China's first civilian hyperspectral service satellite. ZY1-02D is equipped with a 9-band multi-spectral camera and a 166-band hyperspectral camera, including 2.5 m panchromatic, 10 m multi-spectral, and 30 m hyperspectral cameras. The detailed parameters are shown in Table 1. Hyperspectral data can provide more accurate retrieval of standard aquatic products, and this sensor can potentially provide more detailed information about optically active components.

Table 1. ZY1-02D parameter setting.

Parameters	ZY1-02D AHSI	ZY1-02D VNIC
Waveband Range	VNIR: 440–1040 nm SWIR: 1005–2501 nm	B1: 452–521 nm B2: 522–607 nm B3: 635–694 nm B4: 776–895 nm B5: 416–452 nm B6: 591–633 nm B7: 708–752 nm B8: 871–1047 nm
Spectral sampling interval	VNIR: 10 nm SWIR: 20 nm	20–60 nm
Number of bands	166	8
Spatial resolution	30 m	10 m
Width	60 km	115 km

The remote sensing reflectance is the basis of the application of hyperspectral remote sensing data. The hyperspectral reflectance of the ZY1-02D satellite is directly related to the efficiency and quality of applications involving hyperspectral data. The preprocessing of ZY1-02D hyperspectral data mainly includes coincident band elimination, radiometric calibration, and atmospheric correction.

According to the ZY1-02D satellite spectrum settings and the characteristics of the water spectrum curve, the last five bands of the visible near-infrared (NIR) band overlap with the first three bands of the NIR band, so that the redundant bands (77–79) are eliminated, and the total number of bands is 163.

Radiometric calibration is used to establish the quantitative relationship between the radiances of the different wavebands and the original pixel value of the sensor. The equation for the radiometric calibration of remote sensing images is

$$L = Gain \times DN + offset. \quad (2)$$

where L is the apparent radiation measurement value; DN is the original value of the remote sensing image; $Gain$ is the gain value of the absolute radiation calibration coefficient; and $offset$ is the offset value.

The signal detected by the remote sensor is affected by the absorption and scattering caused by atmospheric components (by approximately 90%). These phenomena are one of the uncertain factors in the remote monitoring of the chlorophyll-*a* concentration [23]. The purpose of atmospheric correction is to eliminate atmospheric molecular reflection. The apparent radiance or apparent reflectance after the radiation calibration is inverted into the true reflectance close to the ground object. There are many atmospheric correction methods, which can be divided into absolute atmospheric correction methods and relative atmospheric correction methods, according to their corrected results. The atmospheric radiation transfer model is the most accurate correction method among the many models of absolute atmospheric correction methods, including fast line-of-sight atmospheric analysis of hypercubes (FLAASH), Second Simulation of the Satellite Signal in the Solar Spectrum (6S), and Quick Atmospheric Correction (QUAC) models.

The FLAASH model is suitable for multi-spectral and hyperspectral images and can accurately compensate for atmospheric effects. Its applicable wavelength range is from visible light to NIR and short-wave infrared, with a maximum wavelength of 3 μm . In the moderate resolution atmospheric transmission version 4 (MODTRAN4) model, the atmospheric correction parameters include the satellite transit time, aerosol type, and atmospheric model. The FLAASH model provides three wavebands for water vapor inversion: 1050–1210 nm (1135 nm), 870–1020 nm (940 nm), and 770–870 nm (820 nm). The aerosol optical thickness is dark and is obtained using the pixel inversion method. The use of the MODTRAN standard atmospheric model and the aerosol model to replace real-time atmospheric parameters broadens the application range of the FLAASH model and improves its stability [24].

The 6S model is used to simulate the influence of the atmosphere during the transmission of sunlight from the Sun to the ground target to the sensor. Through simulations, the degree of influence of the atmosphere on the solar radiation can be obtained to carry out atmospheric correction. The latest 6S atmospheric correction code requires auxiliary data, including the moisture content, ozone content, aerosol optical thickness, and terrain height.

The QUAC model is an algorithm based on dark pixels, and it considers three hypotheses. (1) The image must contain more than 10 spectrally different pixels. (2) The standard deviation of the end-member pixel reflectance is spectrally independent and can be used to calculate the transmittance. (3) The existence of a related number of dark pixels is used to calculate the constant baseline, which is assumed to be the measurement of the attenuation (scattering and absorption) and remote sensing. The calculation speed of the atmospheric correction method is significantly faster than that of the method based on the radiation transmission model because the QUAC model does not involve first-principle radiation transmission calculations, and it only requires an approximate description of the sensor band position (the central wavelength) and its radiation calibration.

In this study, the FLAASH module of the ENVI 5.5 software was chosen to perform the atmospheric correction of the water bodies, and atmospheric correction of the ZY1-02D images was carried out after radiation calibration because the aerosols in the study area were not affected by urban or industrial inputs. Due to the strong influence of the source, the rural aerosol model in the FLAASH module and the 2-band (KT) aerosol inversion method were chosen. Figure 2 shows a comparison of the water reflectance data before and after the atmospheric correction for the same pixel and a comparison between the water reflectance after the atmospheric correction and the measured water reflectance. After the FLAASH atmospheric correction, the spectrum of the satellite image retains the major features of the measured spectrum.

3. Methods

3.1. Water Extraction

For small and medium-sized inland lakes, the lake area is greatly affected by the proximity of the land and vegetation [25]. The water body extraction area directly affects the accuracy of the chlorophyll-a inversion of the water body, which leads to distortion of the chlorophyll-a inversion model. Most lake water body methods use masks to solve the neighbor effect. A small mask range will increase the number of land pixels and the uncertainty of the remote sensing reflectance. If the mask range is too large, it will reduce the amount of effective data. The ZY1-02D data were collected using an AHSI sensor with a 30 m spatial resolution and a VNIC sensor with a 10 m spatial resolution.

Based on multi-spectral Landsat data, Mcfeeters proposed the use of the NIR band and the green light band to construct the Normalized Difference Water Index (NDWI) based on a large number of experiments [26]. The definition of the NDWI is

$$\text{NDWI} = \frac{R_{\text{rs}}(\lambda_1) - R_{\text{rs}}(\lambda_2)}{R_{\text{rs}}(\lambda_1) + R_{\text{rs}}(\lambda_2)} \quad (3)$$

where λ_1 is the reflectance in the green light band and λ_2 is the reflectance in the NIR band. The NDWI can quantitatively describe the performance characteristics of the water body in the image, so it can effectively realize the automatic extraction of the water body information. The underlying surface of Baiyangdian Lake is complicated by human activities, and the water area is small and fragmented. Based on the narrow-band water spectrum information about Baiyangdian Lake ZY1-02D, the band combination for the NDWI was determined.

Baiyangdian Lake is an optically shallow water area. The water reflectance curve is shown in Figure 3. In the range of 400–500 nm, due to the strong absorption of blue light by chlorophyll-a and yellow substances, the water reflectance in this wavelength range is generally low. In the range of 510–620 nm, due to the weak absorption of chlorophyll-a and carotene and the scattering of cells and suspended particles, a reflection peak is formed. The size of the reflection peak is related to the pigment composition, and the higher the chlorophyll-a concentration of the water, the larger the peak. Thus, it can be used as a quantitative indicator of the chlorophyll-a concentration. Another reflection peak appears in the range of 685–730 nm. This peak is generally considered to be the fluorescence peak of chlorophyll-a. Its position and reflectivity increase as the chlorophyll-a concentration increases. Displacement occurs in the direction of the longer wavelengths, and this peak is the most prominent feature of algae-bearing water bodies. Its presence or absence is usually used as the basis for judging whether the water contains algae-related chlorophyll-a [27]. The position and value of the reflection peak are important indicators of the chlorophyll-a concentration. Beyond 730 nm, the reflectivity of the water body is relatively low due to the absorption by the water body.

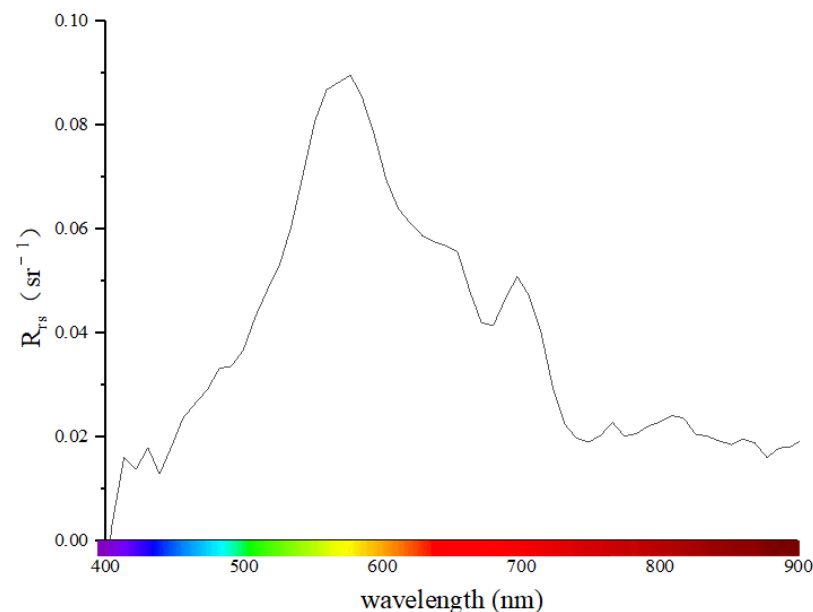


Figure 3. Water spectrum of Baiyangdian Lake.

The NDWI band was determined based on the spectral curve characteristics of the features of Baiyangdian Lake. The reflection peak and absorption valley in Figure 2 correspond to $\lambda_1 = 576$ nm and $\lambda_2 = 730$ nm in the ZY1-02D image. Therefore, the water extraction formula for the ZY1-02D hyperspectral data is

$$NDWI = \frac{R_{rs}(567) - R_{rs}(730)}{R_{rs}(567) + R_{rs}(730)} \quad (4)$$

ZY1-02D is equipped with a multi-spectral sensor with a spatial resolution of 10 nm. The central wavelength of B2 is 555 nm, and the central wavelength of B7 is 725 nm. The water extraction formula for the ZY1-02D multi-spectral data is

$$NDWI = \frac{B2 - B7}{B2 + B7} \quad (5)$$

The multi-spectral data bright surface water extraction results and the hyperspectral bright surface water extraction results were superimposed and analyzed, which effectively eliminated the information about the banks, improved the accuracy of the water extraction, and obtained the water surface distribution of Baiyangdian Lake (Figures 4 and 5).

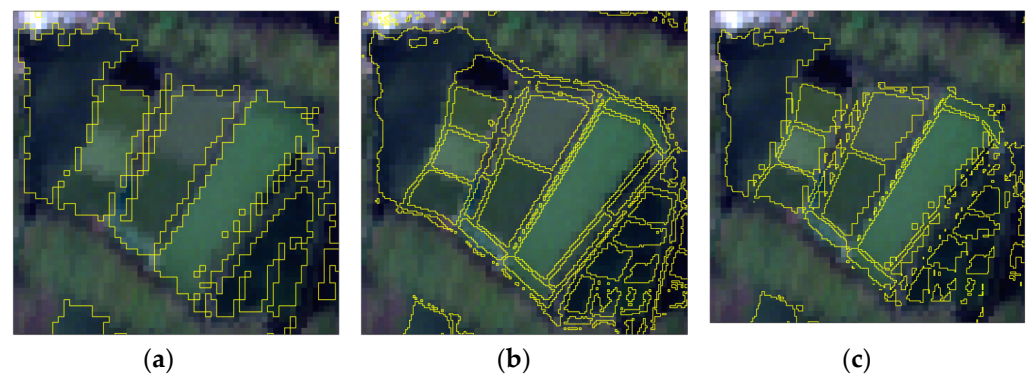


Figure 4. Example of water body extraction, (a) hyperspectral extraction of water surfaces; (b) multi-spectral extraction of water surfaces; (c) body of water after superposition.

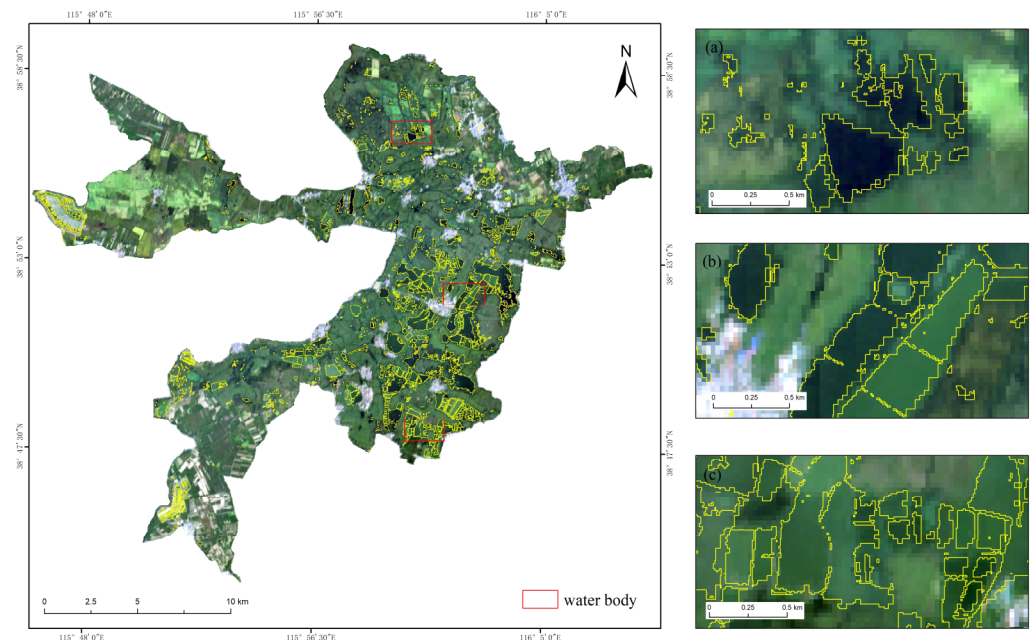


Figure 5. Boundaries of Baiyangdian surface water bodies. (a) Shaochedian Lake; (b) Laowangdian Lake; (c) Mengjiadian Lake.

3.2. Chlorophyll-*a* Model Construction

3.2.1. Screening of Sensitive Bands

Single Band

The correlation coefficients between the chlorophyll-*a* concentration and each band of the ZY1-02D pixel remote sensing reflectivity were calculated and the best band for the

chlorophyll-a concentration inversion was identified. Figure 6 shows that the chlorophyll-a concentration at 400–680 nm is negatively correlated with the reflectance, while the chlorophyll-a concentration at 680–900 nm is positively correlated with the reflectance. The maximum correlation coefficient (0.6518) occurred at 713.79 nm, so the reflection at 713.79 nm was selected. The rate and chlorophyll-a concentration were used for the regression modeling.

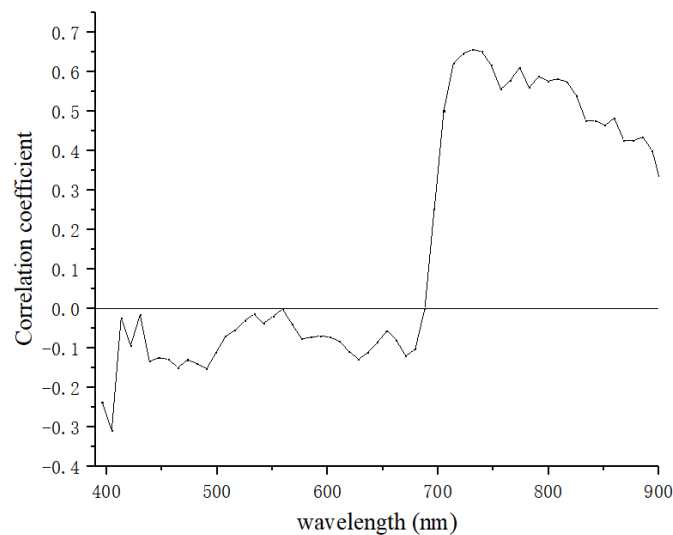


Figure 6. Plot of the correlation coefficient versus wavelength.

Band Calculations

The band ratio model factors in the chlorophyll-a inversion mainly include the blue-green band ratio and the NIR band ratio. Among them, the NIR and red-band ratio models are usually used for optically complex Case-II water bodies, which are mainly affected by the chlorophyll-a concentration, the total suspended solids, and the influence of colored dissolved organic matter. The commonly used NIR and red-band ratio models are $R_{rs}(700)/R_{rs}(670)$, $R_{rs}(719)/R_{rs}(667)$, $R_{rs}(706)/R_{rs}(682)$, and $R_{rs}(708)/R_{rs}(665)$. According to the band characteristics of the ZY1-02D data and the existing band combinations, the SPSS Statistics software (IBM) was used to perform the correlation analysis between the different band combinations and the measured chlorophyll-a concentrations to obtain the best band combination using Equation (6).

$$\text{Chl} - a \propto \frac{R_{rs}(713)}{R_{rs}(645)} \quad (6)$$

Three-Band Model

The three-band model is based on the bio-optical theory for the remote sensing inversion of the Chl-a concentrations in turbid Case-II water bodies [28].

$$\text{Chl} - a \propto [R^{-1}(\lambda_1) - R^{-1}(\lambda_2)] \times R(\lambda_3). \quad (7)$$

The model is based on three assumptions. (1) The backscattering coefficients of the three bands are approximately equal. That is, $b_b(\lambda_1) \approx b_b(\lambda_2) \approx b_b(\lambda_3)$, where $b_b(\lambda_1)$, $b_b(\lambda_2)$, and $b_b(\lambda_3)$ are the backscattering coefficients at λ_1 , λ_2 , and λ_3 , respectively. (2) λ_3 is mainly determined by the absorption coefficient of pure water, and the absorption coefficient of the water components can be ignored. That is, $a_w(\lambda_3) \gg a_d(\lambda_3) + a_{CDOM}(\lambda_3) + b_b(\lambda_3)$, where $a_w(\lambda_3)$, $a_d(\lambda_3)$, and $a_{CDOM}(\lambda_3)$ are the absorption coefficients of pure water, non-pigmented particulate matter, and colored dissolved organic matter at λ_3 , respectively. (3) The absorption coefficients of the non-pigmented particulate matter and

colored dissolved organic matter at λ_1 and λ_2 are approximately equal, and λ_1 is located near the absorption peak of Chl-a. That is, $a_{ph}(\lambda_1) \approx a_{ph}(\lambda_2)$, $a_{CDOM}(\lambda_1) \approx a_{CDOM}(\lambda_2)$, and $a_{ph}(\lambda_1) \gg a_{ph}(\lambda_2)$, where $a_{ph}(\lambda_1)$ and $a_{ph}(\lambda_2)$ are the absorption coefficients of phytoplankton pigment particles at λ_1 and λ_2 , respectively. λ_1 should be located at the peak of a_{ph} according to the principle of the standard three-band model. λ_1 is close to λ_2 , $\lambda_2 \geq 690$ nm, λ_3 is located in the NIR band, and $\lambda_3 \geq 730$ nm.

By analyzing the spectral characteristics of the water in Baiyangdian Lake and the commonly used bands of the three-band model, it was found that when $\lambda_1 = 679$ nm, $\lambda_2 = 705$ nm, and $\lambda_3 = 756$ nm, the measured Chl-a concentration in Baiyangdian had the highest correlation with the model, and the correlation coefficient was 0.7.

Four-Band Model

Due to the complex optical properties of inland eutrophic lakes, the assumptions of the three-band model could not simultaneously hold true. A new NIR band was introduced, i.e., the four-band model, to reduce the effect of the absorption by pure water and non-pigmented particles on the estimation of the Chl-a concentration [27].

$$\text{Chl-a} \propto [R^{-1}(\lambda_1) - R^{-1}(\lambda_2)] * [R^{-1}(\lambda_3) - R^{-1}(\lambda_4)] \quad (8)$$

Based on the characteristics of the spectral curve for the water in Baiyangdian Lake, the selection of the bands in the commonly used four-band model, and the spectral channels of ZY1-02D used, in the study, the best bands were determined to be $\lambda_1 = 679$ nm, $\lambda_2 = 696$ nm, $\lambda_3 = 739$ nm, and $\lambda_4 = 705$ nm through repeated experiments and comparisons.

Normalized Difference Chlorophyll Index (NDCI)

Sachidananda Maisha et al. proposed a novel index for estimating the chlorophyll-a concentration, the Normalized Difference Chlorophyll Index (NDCI) [29]. The NDCI index is constructed by applying the remotely sensed reflectance in both the λ_1 and λ_2 bands (Equation (9)) in a normalized form, which can partially eliminate the effects of the solar altitude angle, atmospheric radiation, and other factors. Among them, λ_1 and λ_2 are chosen at the characteristic spectra and their optical properties are dominated by chlorophyll-a. This also reduces the influence of the other water components to a certain extent.

$$\text{Chl-a} \propto \frac{[R_{rs}(\lambda_2) - R_{rs}(\lambda_1)]}{[R_{rs}(\lambda_2) + R_{rs}(\lambda_1)]} \quad (9)$$

Based on the characteristics of the spectral curve for the water in Baiyangdian Lake and the spectral channels of ZY1-02D used, the best bands were determined to be $\lambda_1 = 662$ nm and $\lambda_2 = 705$ nm through repeated tests and comparisons.

Fluorescence Line Height

The Fluorescence Line Height (FLH) model proposed by Neville and Gower is used to estimate the chlorophyll-a concentrations of various types of water bodies [30], and the basic principle of the FLH found using the model is to use the line connecting the off-water irradiance of the left and right channels of the fluorescence peak to the baseline, to calculate the distance between the off-water irradiance of the fluorescence channel and the baseline (Figure 7), and to establish the correlation between the chlorophyll-a mass concentration and the FLH. Using this method, the correlation between the chlorophyll-a mass concentration and the FLH was established. The FLH model is described by Equation (10):

$$FLH = R_{rs}(\lambda_{max}) - R_{rs}(\lambda_2) - \frac{(\lambda_2 - \lambda_{max})(R_{rs}(\lambda_1) - R_{rs}(\lambda_2))}{\lambda_2 - \lambda_1} \quad (10)$$

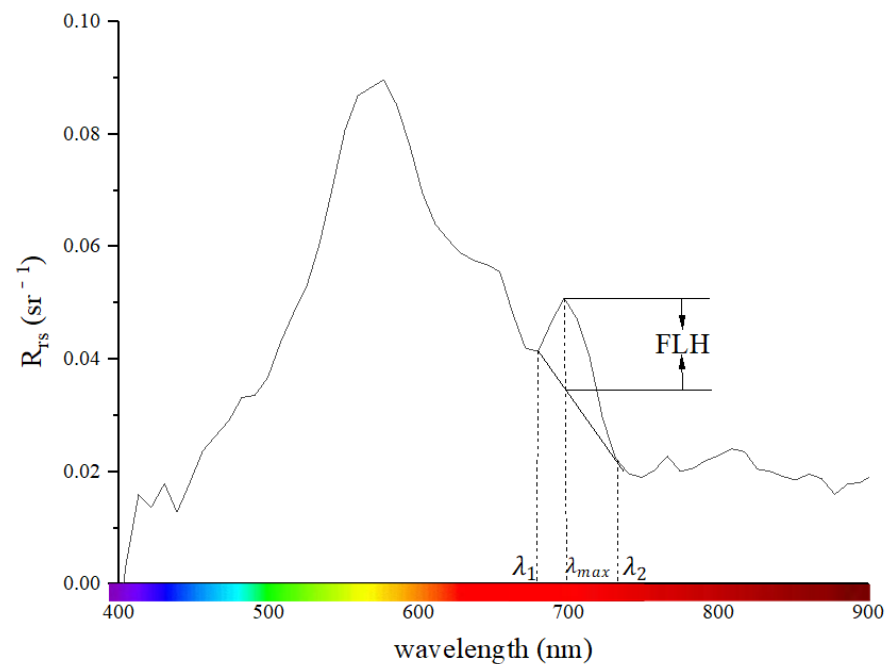


Figure 7. The height of the chlorophyll-a fluorescence peak above the connecting line on both sides.

Based on the spectral curve characteristics of the water in Baiyangdian Lake and the spectral channel of ZY1-02D, $\lambda_{max} = 705$ nm, $\lambda_1 = 679$ nm, and $\lambda_2 = 748$ nm.

According to the above ZY1-02D sensitive band screening, Table 2 was obtained.

Table 2. ZY1-02D sensitive band.

Model	Parameter	λ_1	λ_2	λ_3	λ_4
Single	$R_{rs}(\lambda_1)$	713			
BR	$R_{rs}(\lambda_1)/R_{rs}(\lambda_2)$	645	713		
Three-band	$[R^{-1}(\lambda_1) - R^{-1}(\lambda_2)] \times R(\lambda_3)$	679	705	756	
Four-band	$[R^{-1}(\lambda_1) - R^{-1}(\lambda_2)] * [R^{-1}(\lambda_3) - R^{-1}(\lambda_4)]$	679	696	705	739
NDCI	$\frac{R_{rs}(\lambda_2) - R_{rs}(\lambda_1)}{R_{rs}(\lambda_2) + R_{rs}(\lambda_1)}$	705	662		
FLH	$R_{rs}(\lambda_2) - \left[R_{rs}(\lambda_3) + (R_{rs}(\lambda_1) - R_{rs}(\lambda_3)) \times \frac{R_{rs}(\lambda_3) - R_{rs}(\lambda_2)}{R_{rs}(\lambda_3) - R_{rs}(\lambda_1)} \right]$	679	705	748	

3.2.2. Model Construction

Using the stepwise regression method in the SPSS22 software (gradually eliminating independent variables and increasing the correlation coefficient), a single-band model, ratio model, three-band model, and four-band model were constructed based on the measured Chl-a concentration data and the narrow band of the ZY1-02D AHSI images. The normalized chlorophyll-a difference index and the FLH model were used to establish linear, polynomial, and exponential models. Finally, the fitting equation and R^2 values were obtained.

Figure 8 shows the estimated results of the different models. Among them, the fluorescent line height model has the best estimation accuracy, with $y = 0.028x + 8.023$ and $R^2 = 0.84$.

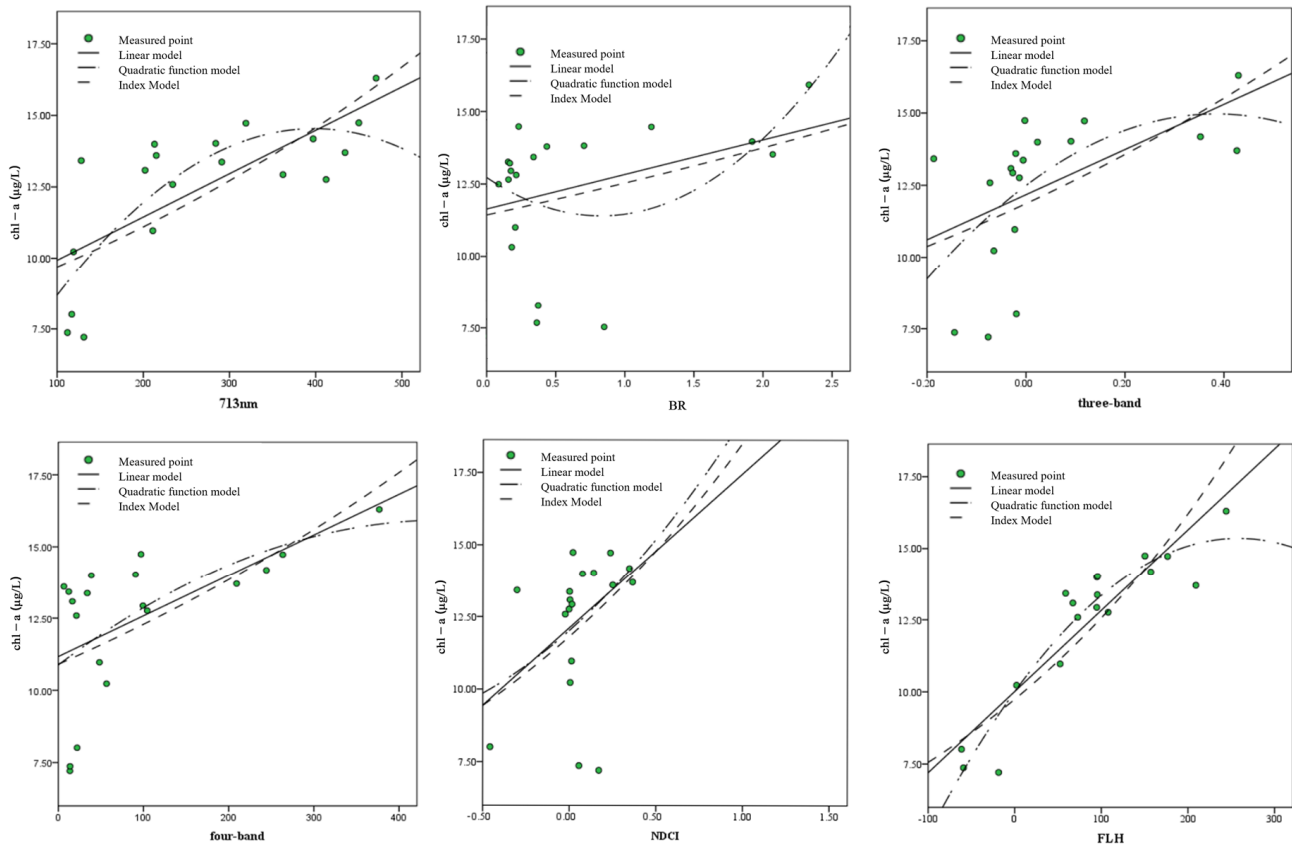


Figure 8. Fitting of the different models to the measured chlorophyll-a concentrations.

3.2.3. Accuracy Assessment

The Leave-One-Out Crossover (LOOCV) method was used to verify the accuracy of the inversion. This verification method has been proven to be effective in evaluating the inductive characteristics of statistical models, and the result is almost unbiased [8]. This method involves taking out one of the N samples s , the remaining $N-1$ samples are used to design the prediction model, and then, the samples taken are used for the testing. This process is repeated N times, the tests are conducted N times, and the average forecast deviation is counted.

The SPSS Statistics (IBM) software was used for all statistical analysis, including calculating the average, maximum, and minimum values, correlation analysis, and linear and non-linear regression. In addition, several indicators were used to evaluate the performance and uncertainty of the algorithm, including (1) the coefficient of determination (R^2), (2) the Root Mean Square Error (RMSE), and (3) the Mean Absolute Percentage Error (MAPE). Among them, the R^2 value represents the degree of correlation between the coupled data. The RMSE represents the difference between the predicted value and the actual value, and a smaller RMSE indicates a higher prediction accuracy. The MAPE is used to measure the accuracy of the prediction, and a smaller MAPE value indicates a better modeling result. These accuracy standards are defined in Equations (11) and (12).

$$RMSE = \sqrt{\frac{1}{n} \sum_{i=1}^n (Chl_{-a_i} - Chl_{-a'_i})^2} \quad (11)$$

$$MAPE = \frac{1}{n} \sum_{i=1}^n \left| \frac{Chl_{-a_i} - Chl_{-a'_i}}{Chl_{-a_i}} \right| \times 100\%. \quad (12)$$

where n is the number of samples, and Chl_{-a_i} and $Chl_{-a'_i}$ are the measured and predicted Chl-a concentrations.

4. Results

4.1. Model Validation

Based on the ground-truth (i.e., measured) Chl-a concentrations and the satellite spectral profiles of the corresponding image elements, the inverse model construction and accuracy validation were carried out using the five models introduced in Section 3.2. The obtained model formulas, R^2 values, and error indexes of the validation set are presented in Table 3.

Table 3. Model validation.

Name	Model	R^2	RMSE ($\mu\text{g/L}$)	MAPE
Single	$y = 0.015x + 4.415$	0.55	25.97	24.69%
BR	$y = -1.667x^2 + 7.412x + 3.8777$	0.75	20.22	18.16%
Three-band	$y = 7.814x + 2.023$	0.66	17.89	17.78%
Four-band	$y = 10.907e^{0.01x}$	0.52	24.66	29.27%
NDCI	$y = 5.344x^2 - 2.007x + 12.03$	0.70	19.57	29.17%
FLH	$y = 0.028x + 8.023$	0.78	15.55	16.31%

The RMSE of the fluorescence height model was $15.55 \mu\text{g/L}$, and the MAPE was 16.31%. Figure 9 shows that the scatter points of the measured and inverse Chl-a concentrations were evenly distributed on both sides of the 1:1 line, indicating that the constructed FLH model can be used to invert the Chl-a concentration of Baiyangdian Lake.

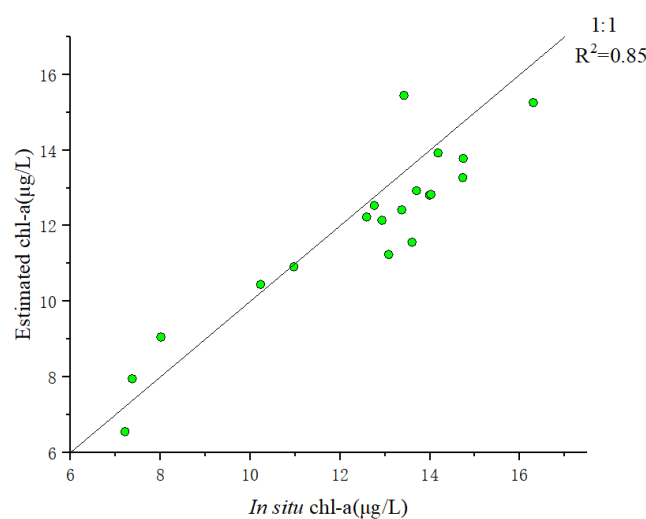


Figure 9. Scatter plot of in situ versus ZY1-02D-derived Chl-a concentrations.

4.2. Inverted Chlorophyll-a Results

Based on the FLH model, the chlorophyll-a concentrations of the Baiyangdian water bodies were inverted, and the distribution of the chlorophyll-a concentration in Baiyangdian Lake was obtained. The maximum value of the inversion results was $15.40 \mu\text{g/L}$, and the minimum value was $2.05 \mu\text{g/L}$. Figure 10a–c shows the spatial distribution of the chlorophyll-a concentration in Baiyangdian. The difference in the chlorophyll-a concentrations in different areas was obvious, as well as the establishment of a wet-land in the inlet of Fu River. The natural reserve at the mouth of the Fuhe River was established to purify the water, the chlorophyll-a concentration was low, and the water quality was good. The spatial distribution of chlorophyll-a concentrations in Shaoche Lake and Laowang Lake shows a low center and high level on both sides. Jinlong Lake has fishponds and perimeter dikes. Figure 10 shows that the chlorophyll-a concentrations of the fishponds inside the perimeter dike were significantly different from those outside the perimeter dike, and the chlorophyll-a concentrations of the fishponds were lower after treatment than before

treatment, indicating at the spatial distribution of the chlorophyll-a concentration in the study area based on the inversion of ZY1-02D hyperspectral data is relatively reasonable.

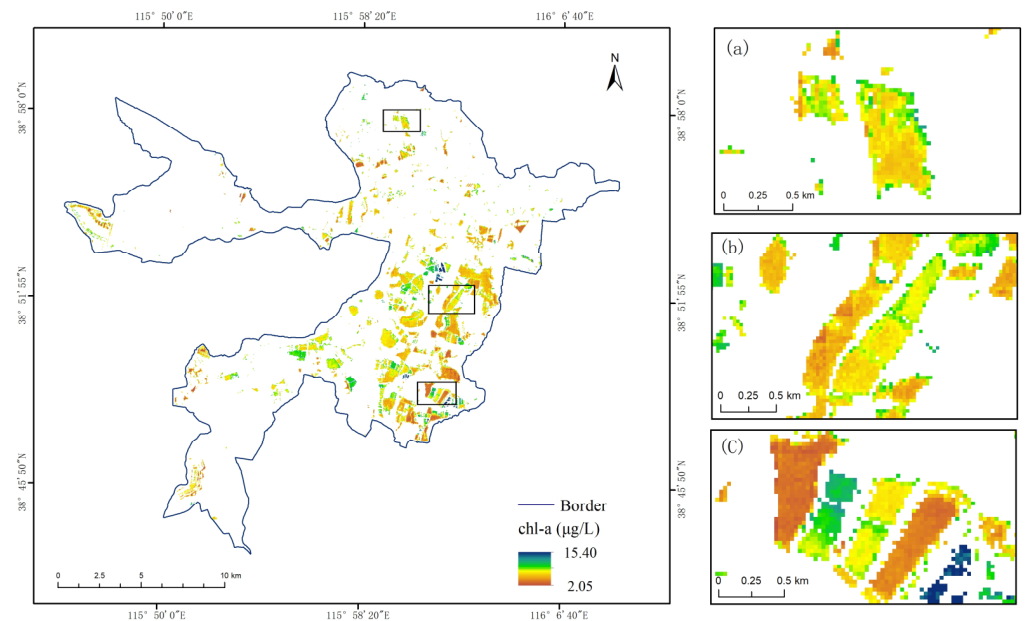


Figure 10. Results of the chlorophyll-a inversion for Baiyangdian Lake. (a) Shaochedian Lake; (b) Laowangdian Lake; (c) Jinlongdian Lake.

5. Discussion

5.1. ZY1-02 -Based and Sentinel-Based Chl-a Products

Sentinel-2 carries a high spatial (10–20 m) and temporal (2–3 days) resolution of MSI and contains a sensitive “red-edge band”, which is a sensitive band for inversion of chlorophyll-a concentration by fluorescence line height model. In this study, the sentinel-2 data on 4 October 2020 were selected, and the hyperspectral inversion model (FLH) was applied to the sentinel-2 data to obtain the sentinel-2 multispectral inversion results. The inversion results were simulated and verified with the inversion results of the measured chlorophyll-a concentration, and the verification $R^2 = 0.66$ was obtained (Figure 11). This further illustrates the advantage of hyperspectral inversion of chlorophyll-a concentration.

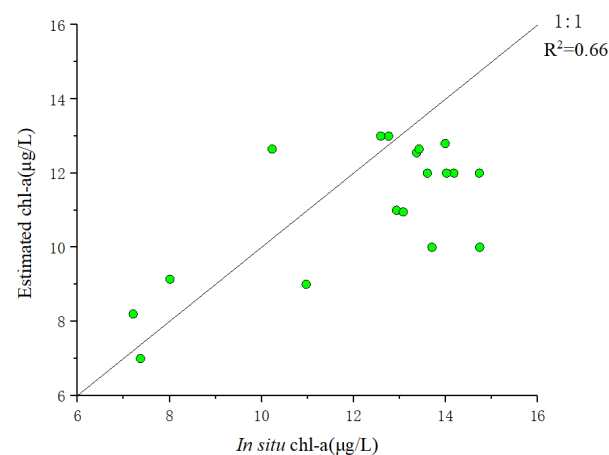


Figure 11. Scatter plot of in situ versus sentinel-2-derived Chl-a concentrations.

5.2. Uncertainties and Limitations

In this study, there are two main factors to improve the accuracy of chlorophyll-a concentration assessment in Baiyangdian: the advantage of the spectral resolution of ZY1-

02D and the chlorophyll-a concentration dataset of simultaneous measurements. However, there are limitations in the model assessment. First, the acquisition of the chlorophyll-a dataset is mainly focused on autumn, the next step needed is to acquire synchronous chlorophyll-a concentration datasets in spring and summer by star field to validate the model. Second, it is found that the chlorophyll-a inversion results obtained using ZY1-02D data are affected by the image noise and remote sensing reflectance accuracy. The image-based remote sensing reflectance estimation method for water surface in this study produced good results, but more accurate remote sensing reflectance acquisition is needed, which will further improve the accuracy of chlorophyll-a concentration inversion. Further development of the high-precision atmospheric correction method for ZY1-02D water body images is also needed. Finally, due to the long revisit period (approximately 55 days) and low temporal resolution of the ZY1-02D single star, it is difficult to meet the demand for multi-frequency water monitoring, the next work can increase the time series with the help of multispectral image data.

6. Conclusions

The spectral resolution of ZY1-02D is 10 nm within 400–900 nm. Its high spectral resolution is more likely to reflect the sensitive spectrum of the water-color absorption and reflection characteristics and to achieve high-precision chlorophyll-a concentration inversion. In this study, ZY1-02D hyperspectral data and multi-spectral data were used to clarify the surface water area to obtain the clear water surface area in Baiyangdian and to monitor and evaluate the chlorophyll-a concentration of the open water in Baiyangdian at the optimal wavelength band. Then, based on the semi-empirical method for determining the Baiyangdian chlorophyll-a concentration, multi-model regression fitting was performed. Finally, the FLH model was determined as having the highest inversion accuracy. Applying the inversion model to Baiyangdian Lake and its evaluation improved the inversion accuracy of the chlorophyll-a concentration of the water bodies, and becomes of great significance for the monitoring and evaluation of the chlorophyll-a concentrations of the Baiyangdian water bodies.

Author Contributions: Conceptualization, L.L. and Z.G.; methodology, L.L.; software, L.L.; validation, L.L., Z.G., Y.L. and S.L.; formal analysis, Y.L. and S.L.; investigation, S.L. and Y.L.; writing—original draft preparation, S.L.; writing—review and editing, Z.G.; supervision, Z.G.; project administration, Z.G.; funding acquisition, Z.G. All authors have read and agreed to the published version of the manuscript.

Funding: This research was funded by the National Natural Science Foundation of China (Grant No. 41971381) and the Key Program of Beijing Municipal Bureau of Water (Grant No. TAHP-2018-ZBYY-490S).

Acknowledgments: The authors would like to thank the Department of Natural Resources Satellite Remote Sensing Cloud Service Platform for the ZY1-02D hyperspectral data, the ESA for the Sentinel-2 data. The authors thank the anonymous reviewers for their constructive comments on our manuscript.

Conflicts of Interest: The authors declare no conflict of interest.

References

1. Neil, C.; Spyarakos, E.; Hunter, P.D.; Tyler, A.N. A global approach for chlorophyll-a retrieval across optically complex inland waters based on optical water types. *Remote Sens. Environ.* **2019**, *229*, 159–178. [[CrossRef](#)]
2. Sagan, V.; Peterson, K.T.; Maimaitijiang, M.; Sidike, P.; Sloan, J.; Greeling, B.A.; Maalouf, S.; Adams, C. Monitoring inland water quality using remote sensing: Potential and limitations of spectral indices, bio-optical simulations, machine learning, and cloud computing. *Earth-Sci. Rev.* **2020**, *205*, 103187. [[CrossRef](#)]
3. Guo, M.; Li, J.; Sheng, C.; Xu, J.; Wu, L. A Review of Wetland Remote Sensing. *Sensors* **2017**, *17*, 777. [[CrossRef](#)] [[PubMed](#)]
4. Liu, X.; Steele, C.; Simis, S.; Warren, M.; Tyler, A.; Spyarakos, E.; Selmes, N.; Hunter, P. Retrieval of Chlorophyll-a concentration and associated product uncertainty in optically diverse lakes and reservoirs. *Remote Sens. Environ.* **2021**, *267*, 112710. [[CrossRef](#)]
5. Smith, M.E.; Lain, L.R.; Bernard, S. An optimized Chlorophyll a switching algorithm for MERIS and OLCI in phytoplankton-dominated waters. *Remote Sens. Environ.* **2018**, *215*, 217–227. [[CrossRef](#)]

6. Zhang, G.; Yao, T.; Chen, W.; Zheng, G.; Shum, C.K.; Yang, K.; Piao, S.; Sheng, Y.; Yi, S.; Li, J.; et al. Regional differences of lake evolution across China during 1960s–2015 and its natural and anthropogenic causes. *Remote Sens. Environ.* **2019**, *221*, 386–404. [[CrossRef](#)]
7. Guan, Q.; Feng, L.; Hou, X.; Schurgers, G.; Zheng, Y.; Tang, J. Eutrophication changes in fifty large lakes on the Yangtze Plain of China derived from MERIS and OLCI observations. *Remote Sens. Environ.* **2020**, *246*, 111890. [[CrossRef](#)]
8. Feng, L.; Hu, C.; Han, X.; Chen, X.; Qi, L. Long-Term Distribution Patterns of Chlorophyll-a Concentration in China's Largest Freshwater Lake: MERISFull-Resolution Observations with a Practical Approach. *Remote Sens.* **2015**, *7*, 275–299. [[CrossRef](#)]
9. Jiang, G.; Loiselle, S.A.; Yang, D.; Ma, R.; Gao, C. Remote estimation of chlorophyll a concentrations over a wide range of optical conditions based on water classification from VIIRS observations. *Remote Sens. Environ.* **2020**, *241*, 111735. [[CrossRef](#)]
10. Bi, S.; Li, Y.; Liu, G.; Song, K.; Lyu, H. Assessment of Algorithms for Estimating Chlorophyll-a Concentration in Inland Waters: A Round-Robin Scoring Method Based on the Optically Fuzzy Clustering. *IEEE Trans. Geosci. Remote* **2021**, *60*, 1–17. [[CrossRef](#)]
11. Du, C.; Wang, S.; Zhou, Y.; Yan, F. Retrieval of Chlorophyll a Concentration in Lake Taihu by Three-band Method Using Hyperion Hyperspectral Data. *Environ. Sci.* **2009**, *30*, 7.
12. Yin, Z.; Li, J.; Fan, H.; Gao, M.; Xie, Y. Preliminary Study on Water Quality Parameter Inversion for the Yuqiao Reservoir Based on Zhuhai-1 Hyperspectral Satellite Data. *Spectrosc. Spectr. Anal.* **2021**, *41*, 5.
13. Pahlevan, N.; Smith, B.; Schalles, J.; Binding, C.E.; Stumpf, R. Seamless retrievals of chlorophyll-a from Sentinel-2 (MSI) and Sentinel-3 (OLCI) in inland and coastal waters: A machine-learning approach. *Remote Sens. Environ.* **2020**, *240*, 111604. [[CrossRef](#)]
14. Wang, X.; Gong, Z.; Pu, R. Estimation of chlorophyll-a content in inland turbidity waters using WorldView-2 imagery: A case study of the Guanting Reservoir, Beijing, China. *Environ. Monit. Assess* **2018**, *190*, 620. [[CrossRef](#)] [[PubMed](#)]
15. Gai, Y.; Yu, D.; Zhou, Y.; Yang, L.; Chen, J. An Improved Model for Chlorophyll-a Concentration Retrieval in Coastal Waters Based on UAV-Borne Hyperspectral Imagery: A Case Study in Qingdao, China. *Water* **2020**, *12*, 2769. [[CrossRef](#)]
16. Bramich, J.; Fischer, A.; Bolch, C. Improved red-edge chlorophyll-a detection for Sentinel 2. *Ecol. Indic.* **2021**, *120*, 106876. [[CrossRef](#)]
17. Cao, Z.; Ma, R.; Duan, H.; Pahlevan, N.; Melack, J.; Shen, M.; Xue, K. A machine learning approach to estimate chlorophyll-a from Landsat-8 measurements in inland lakes. *Remote Sens. Environ.* **2020**, *248*, 111974. [[CrossRef](#)]
18. Sun, W.; Yang, G.; Chen, C.; Chang, M.; Huang, K.; Meng, X.; Liu, L. Development status and literature analysis of China's earth observation remote sensing satellites. *J. Remote Sens.* **2020**, *24*, 32.
19. Zhu, J.; Zhou, Y.; Wang, S.; Wang, L.; Liu, W.; Li, H.; Mei, J. Ecological function evaluation and regionalization in Baiyangdian Wetland. *Acta Ecol. Sin.* **2020**, *40*, 14.
20. Yi, Y.; Lin, C.; Tang, C. Hydrology, environment and ecological evolution of Lake Baiyangdian since 1960s. *J. Lake Sci.* **2020**, *32*, 1333–1347.
21. Zhao, Y.; Wang, S.; Zhang, F.; Shen, Q.; Li, J.; Yang, F. Remote Sensing-Based Analysis of Spatial and Temporal Water Colour Variations in Baiyangdian Lake after the Establishment of the Xiong'an New Area. *Remote Sens.* **2021**, *13*, 1729. [[CrossRef](#)]
22. Junwu, T.; Guoliang, T.; Xiaoyong, W.; Xiaomei, W.; Qingjun, S. The Methods of Water Spectra Measurement and Analysis I: Above-Water Method. *J. Remote Sens.* **2004**, *8*, 8.
23. Vanhellemont, Q.; Ruddick, K. Advantages of high quality SWIR bands for ocean colour processing: Examples from Landsat-8. *Remote Sens. Environ.* **2015**, *161*, 89–106. [[CrossRef](#)]
24. Wang, D.; Ma, R.; Xue, K.; Loiselle, S. The Assessment of Landsat-8 OLI Atmospheric Correction Algorithms for Inland Waters. *Remote Sens.* **2019**, *11*, 169. [[CrossRef](#)]
25. Li, D.; Wu, B.; Chen, B.; Xue, Y.; Zhang, Y. Review of water body in formation extraction based on satellite remote sensing. *J. Tsinghua Univ.* **2020**, *60*, 15.
26. Mcfeeters, S.K. The use of the Normalized Difference Water Index (NDWI) in the delineation of open water features. *J. Remote Sens.* **1996**, *17*, 1425–1432. [[CrossRef](#)]
27. Matsushita, B.; Yang, W.; Yu, G.; Oyama, Y.; Yoshimura, K.; Fukushima, T. A hybrid algorithm for estimating the chlorophyll-a concentration across different trophic states in Asian inland waters. *ISPRS J. Photogramm. Remote Sens.* **2015**, *102*, 28–37. [[CrossRef](#)]
28. Tian, H.; Cao, C.; Xu, M.; Zhu, Z.; Liu, D.; Wang, X.; Cui, S. Estimation of chlorophyll-a concentration in coastal waters with HJ-1A HSI data using a three-band bio-optical model and validation. *Inter. J. Remote Sens.* **2014**, *35*, 5984–6003. [[CrossRef](#)]
29. Mishra, S.; Mishra, D.R. Normalized difference chlorophyll index: A novel model for remote estimation of chlorophyll-a concentration in turbid productive waters. *Remote Sens. Environ.* **2012**, *117*, 394–406. [[CrossRef](#)]
30. Luo, J.; Qin, L.; Mao, P.; Xiong, Y.; Zhao, W.; Gao, H.; Qiu, G. Research Progress in the Retrieval Algorithms for Chlorophyll-a, a Key Element of Water Quality Monitoring by Remote Sensing. *Remote Sens. Technol. Appl.* **2021**, *36*, 473–488.